Theor Chem Acc (2011) 129:833–845
DOI 10.1007/s00214-011-0942-8

REGULAR ARTICLE

# Theoretical study on photophysical properties of 2,1,3-benzothiadiazole-based star-shaped molecules

**Ying-Fang Liu · Xue-Feng Ren · Lu-Yi Zou · Ai-Min Ren · Ji-Kang Feng · Chia-Chung Sun**

Received: 1 January 2011 / Accepted: 11 April 2011 / Published online: 28 April 2011


**Abstract** Star-shaped molecules with tailoring functional groups in the core and the arms have great potential application in organic light-emitting devices, because it can be designed to realize low band gap, broad absorption, and excellent solubility for low-cost solution process. To gain an insight into the structure–property relationships, a set of four-arm star-shaped molecules with 2,1,3-benzothiadiazole as the core, different $\pi$-conjugated groups as the arm, and triphenylamine or 2-(pyridin-2-yl) pyridine as the end-group were designed. In this study, a systematic investigation into them was carried out using the density functional theory and time-dependent density functional theory methods. The calculated ionization potentials, electron affinities, and reorganization energies ($\lambda$) show that the properties of the $\pi$-conjugated bridge and the end-group significantly affect the carrier injection and transport characteristics of these molecules, especially for S-BTDP and S-EBTD. Among these molecules, S-BTDP exhibits better electron injection ability due to the introduction of 2-(pyridin-2-yl) pyridine as the end-group. However, S-EBTD, with ethylene as $\pi$-conjugated bridge, has excellent hole injection and carrier transport behaviors. We also calculated the singlet-to-triplet exciton-formation cross-section ratio ($\sigma_S/\sigma_T$), the exciton-formation fractions ($\chi_S$), and the absorption and emission spectra of these molecules. We calculated that $\sigma_S/\sigma_T$ ranges from 1.78 to 2.76 and that $\chi_S$ is ca. 0.37–0.48. These molecules have two absorption bands in the range of 340–410 nm and 500–613 nm, respectively. The calculated emission spectra range from 619 to 706 nm. It can be deduced that the studied 2,1,3-benzothiadiazole-based star-shaped molecules can serve as efficient red light-emitting electroluminescent materials.

**Keywords** Ionization potential and electron affinity · Reorganization energy · Carrier injection and transport · Exciton-formation fractions · 2,1,3-benzothiadiazole-based star-shaped molecules

## 1 Introduction

Organic light-emitting diodes (OLEDs) based on either small molecules or polymers have been drawing wide attention due to their potential applications in full-color, flexible flat-panel displays and lighting, etc. [1]. Many new materials with RGB (red, green, blue) emission have been developed to meet the requirement of full-color displays [2, 3]. To date, the green and blue emitters have basically met the requirements for the commercial application. Nevertheless, achieving pure red emitter with high quantum efficiency is still a great challenge in this field [4–7]. The red light-emitting organic materials that possess narrow band gap are usually composed of the molecules bearing a strong donor–acceptor substituent or with extended $\pi$ conjugation, or strong intramolecular charge transfer (ICT) character [8–11]. Li et al. [12] synthesized a set of four-arm star-shaped molecules whose emission peaks are located at 660–740 nm as saturated red emission and considered that these molecules can be used in bulk heterojunction organic solar cells (OSCs); meanwhile, their linear counterparts were synthesized for comparison. They found several advantages of these star-shaped molecules, such as monodispersity, excellent solubility, and vast structures with

Y.-F. Liu · X.-F. Ren · L.-Y. Zou · A.-M. Ren (✉) · J.-K. Feng · C.-C. Sun
State Key Laboratory of Theoretical and Computational Chemistry, Institute of Theoretical Chemistry, Jilin University, 130023 Changchun, China
e-mail: aimin_ren@yahoo.com

different functional groups. Furthermore, with tailoring functional groups in the core and the arms, star-shaped molecules can be designed to realize low band gap, broad absorption, and excellent solubility for low-cost solution process [13–21]. Such easily modified structure and the excellent performance shown in the experiment of star-shaped molecules just meet the requirements of the red light-emitting organic materials, which inspired us to design a set of star-shaped molecules with excellent photophysical properties.

Taking into account these problems, we use benzothiodiazole (BTD) core as the electron acceptor, introducing triphenylamine (TPA) into four positions 4, 5, 6, and 7 of benzothiadiazole as the electron donor, and different $\pi$-conjugated chains as $\pi$-bridge connecting the TPA and BTD units, and constructed a set of star-shaped molecules with D-$\pi$-A-$\pi$-D push–pull structure. They are S-BTD (only one thiophene as $\pi$-bridge connecting TPA and BTD unit), S-TBTD, S-EBTD, S-ABTD, and S-SBTD (containing one more thiophene, ethylene, acetylene, and styrene unit in each $\pi$ moiety than S-BTD) (see Fig. 1). At the same time, a two-arm linear molecule based on the 4, 7-positions of benzothiadiazole, namely, L-BTD, is also investigated for comparison. In addition, we use 2-(pyridin-2-yl) pyridine, which is a good acceptor [22], instead of the triphenylamine in S-BTD, to design another star-shaped molecule named S-BTDP, and hope that using 2-(pyridin-2-yl) pyridine as end-group can improve the electron injection capability. To rationalize the experimentally observed properties of known materials and to predict those of unknown ones, density functional theory (DFT), time-dependent density functional theory (TD-DFT), and singles configuration interaction (CIS) calculations have been carried out for the structural, electronic, and optical properties. Ionization potentials (IPs), electron affinities (EAs), reorganization energies ($\lambda$), radiative lifetimes ($\tau$), singlet-to-triplet exciton-formation cross-section ratio ($\sigma_S/\sigma_T$), singlet exciton-formation fractions ($\chi_S$), and the electronic spectra are obtained and discussed in detail. Particular attention was paid to the influence of different $\pi$-conjugated bridge and end-group substituent on the photophysical properties of these materials. It has been shown that these compounds, especially the designed molecules S-EBTD and S-BTDP, can function as efficient red light-emitting materials.

## 2 Computational details

Hybrid GGA functional, Becke's three-parameter (B3) hybrid exchange functional, incorporating the correlation functionals of Lee, Yang and Parr (LYP), namely B3LYP, have become extraordinarily popular, so B3LYP was chosen to optimize the ground-state geometries of these molecules with 6-31G(d) basis set. On the basis of the ground-state geometries, TD B3LYP/6-31G(d) was used to calculate the absorption spectra. The calculated HOMO, LUMO energies, HOMO–LUMO gap, IP(v), EA(v) (v: at the geometry of the neutral molecule), and the maximal absorption wavelength of a representative molecule S-BTD are listed in Table 1; there are also some important experimental data for comparison. As can be seen from Table 1, the maximal absorption wavelengths of S-BTD calculated using B3LYP functional (659 nm) are larger than the experimental data (526 nm) by 133 nm. This may be attributed to the incorrect asymptotic behavior of B3LYP functional for systems containing intramolecular charge transfer [23]. However, as mentioned in introduction, the molecules in this paper precisely possess D-$\pi$-A-$\pi$-D push–pull structure and demonstrate strong charge transfer. For this reason, we adopted the MPW1B95 functional, which is suitable for general applications in covalent and noncovalent thermochemistry, and can give good performance especially for hydrogen bonding, weak interaction, and charge transfer calculations [24].

To compare these two methods, MPW1B95 level with 6-31G(d) basis set was also used to optimize the ground-state geometry of S-BTD. The HOMO and LUMO energies, HOMO–LUMO gap, IP(v), EA(v), and the maximal absorption wavelength obtained are also listed in Table 1. Meanwhile, some important interring distances and dihedral angles of ground-state geometries obtained from B3LYP and MPW1B95 methods are summarized in Table 2 for comparison. Configuration interaction singles (CIS) level with 6-31G(d) basis set was employed to optimize the excited-state geometry of S-BTD. On the basis of their respective excited-state geometries, both TD B3LYP/6-31G(d) and TD MPW1B95/6-31G(d) were used to calculate the fluorescence spectra, and the data obtained are listed in Table 1.

It can be seen from Tables 1 and 2 that the MPW1B95/6-31G(d) method obtained shorter interring distances and smaller dihedral angles in the optimization of ground-state geometry compared with B3LYP/6-31G(d). That is, the ground-state geometry optimized by MPW1B95 functional possesses much better planarity. In addition, the MPW1B95/6-31G(d) method identified lower HOMO energy and higher LUMO energy and, thus, obtained a wider HOMO–LUMO gap, which corrected the overestimate of the maximal absorption wavelength by B3LYP functional. Therefore, the maximal absorption wavelength (564 nm) obtained by MPW1B95/6-31G(d) is much closer to the experimental data (526 nm). Moreover, the emission wavelength obtained by TD B3LYP/6-31G(d) and TD MPW1B95/6-31G(d) are 789 and 689 nm, respectively; while the former is 99 nm larger than the experimental value (690 nm), the latter is almost equal to the

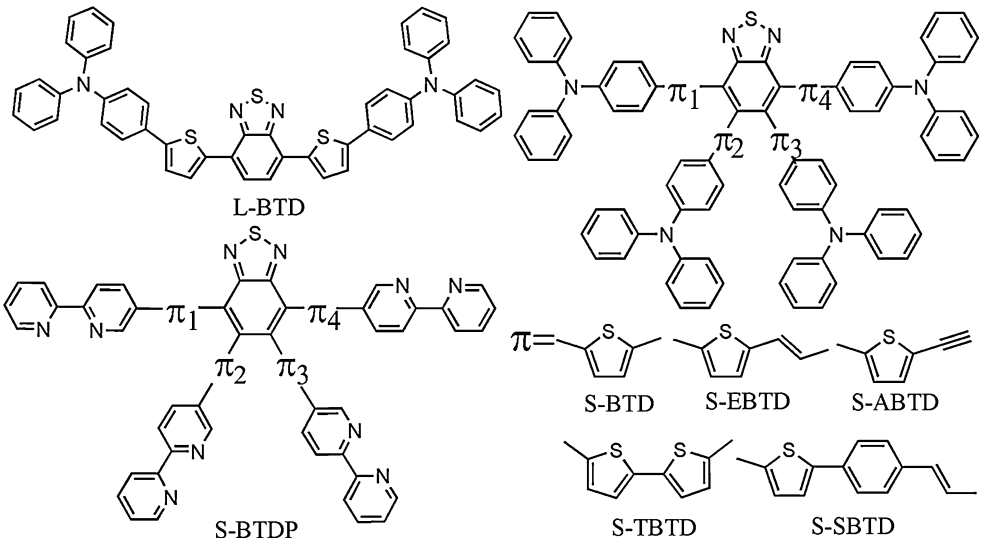


**Fig. 1** Sketch map of the structures for the studied molecules

**Table 1** Negative of the HOMO (-εHOMO) and LUMO (-εLUMO) energies, HOMO–LUMO gaps, ionization potentials (IP) and electronic affinities (EA), maximal absorption and emission wavelengths of S-BTD obtained by B3LYP/6-31G(d) and MPW1B95/6-31G(d) calculations, respectively

| Functional | -εHOMO (eV) | -εLUMO (eV) | $\Delta E_{H-L}$ (eV) | IP(v) (eV) | EA(v) (eV) | $\lambda_{max}^{abs}$ (nm) | $\lambda_{max}^{em}$ (nm) |
|---|---|---|---|---|---|---|---|
| B3LYP | 4.72 | 2.48 | 2.24 | 5.40 | 1.44 | 659 | 789 |
| MPW1B95 | 5.02 | 2.16 | 2.86 | 5.62 | 1.34 | 564 | 689 |
| Exp[a] | 5.45 | | | | | 526 | 690 |

The suffixes (v) indicate vertical values

[a] Li et al. [12]

**Table 2** Interring distances and dihedral angles of the two adjacent moieties D and π, π and A for S-BTD calculated by B3LYP/6-31G(d) and MPW1B95/6-31G(d)

| Method | Interring distances (Å) and dihedral angles (°) | | | | | | | |
|---|---|---|---|---|---|---|---|---|
| | D-$\pi_1$ | $\pi_1$-A | A-$\pi_4$ | $\pi_4$-D | D-$\pi_2$ | $\pi_2$-A | A-$\pi_3$ | $\pi_3$-D |
| B3LYP | 1.465 | 1.468 | 1.468 | 1.465 | 1.465 | 1.485 | 1.485 | 1.466 |
| | 26.2 | 38.6 | 38.8 | 26.3 | 23.9 | 69.5 | 70.0 | 25.3 |
| MPW1B95 | 1.457 | 1.459 | 1.459 | 1.457 | 1.459 | 1.474 | 1.474 | 1.458 |
| | 20.7 | 35.2 | 37.7 | 22.5 | 10.8 | 62.6 | 63.8 | 12.4 |

*D* Triphenylamine (2-(pyridin-2-yl)pyridine for S-BTDP)

π π-conjugated bridge

*A* Benzothiadiazole

experimental value. In summary, MPW1B95 combined with 6-31G(d) method is more suitable for our system than B3LYP/6-31G(d) method obviously.

In this case, the ground-state geometries, as well as their ionic structures of all the molecules in this study were optimized at MPW1B95 level with 6-31G(d) basis set. The IPs, EAs, hole extraction potential (HEP), and electron extraction potential (EEP) were calculated by DFT/MPW1B95 method based on the optimized geometry of the neutral and ionic molecules. On the basis of the ground-state geometries obtained from HF/6-31G(d), we optimized the excited-state geometries of these molecules by CIS level with 6-31G(d) basis set. The absorption and fluorescence spectra were calculated by TD MPW1B95/6-31G(d) on the basis of ground-state and excited-state geometries, respectively. All these calculations were performed on the SGI origin 2000 server with the Gaussian 03 program package [25].

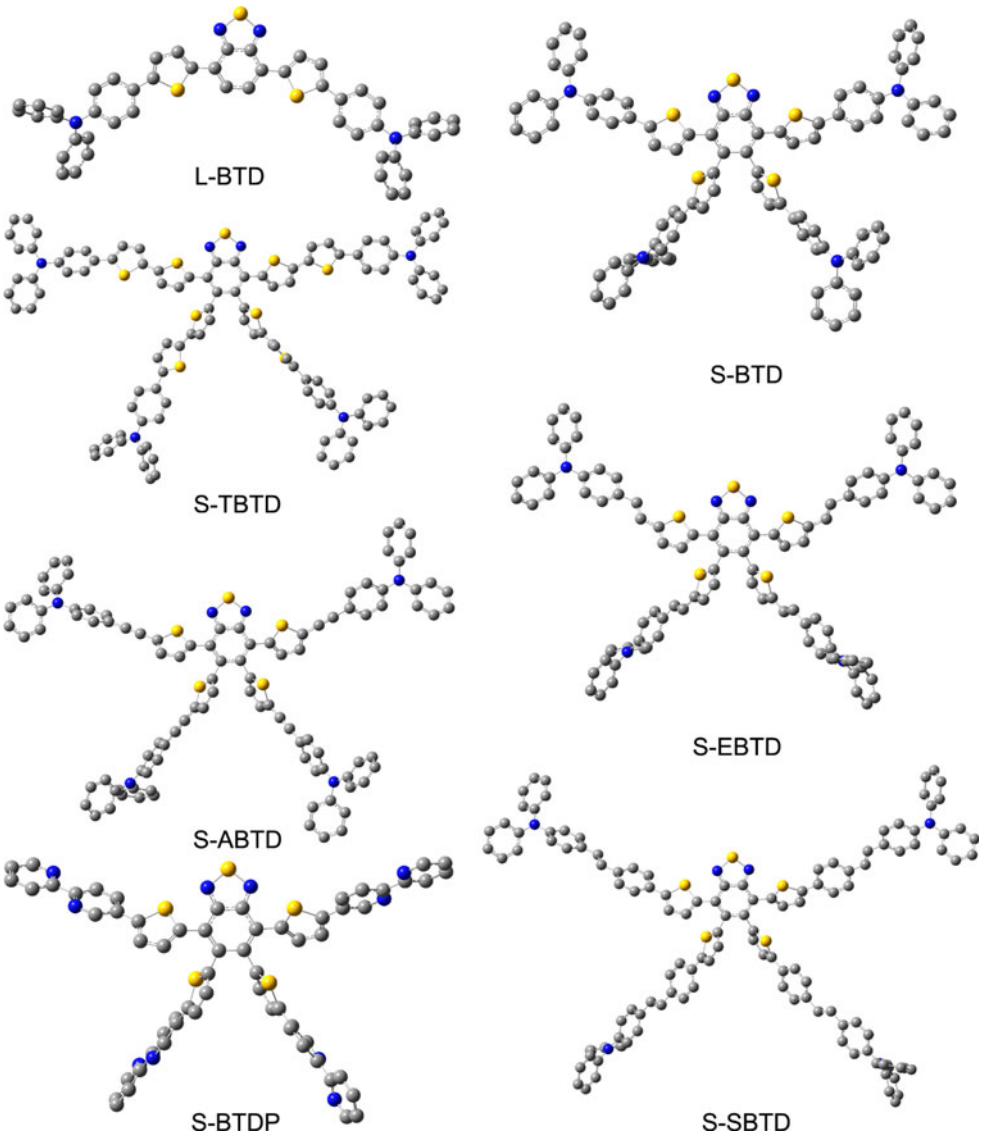


**Fig. 2** Optimized geometries of the studied molecules by MPW1B95/6-31G(d)

## 3 Results and discussion

### 3.1 Ground-state and excited-state geometries

The optimized ground-state geometries of these molecules calculated by MPW1B95/6-31G(d) are depicted in Fig. 2. Some important interring distances and dihedral angles of these molecules in the ground geometries are collected in Tables 3 and 4.

As shown in Table 3, the interring distances of the two adjacent moieties $\pi$ and D of these molecules are similar with each other except S-ABTD. The interring distances between the two adjacent moieties $\pi$ and D of S-ABTD is shorter than others around 0.04 Å in these regions; this can be attributed to the strong attraction of acetylene group to the lone electron pair on nitrogen atom of the electron-donor triphenylamine (TPA). Different from above situation, the interring distances between the two adjacent moieties $\pi$ and A can be divided into two groups by the different geometric environment of $\pi$-conjugated bridge. Moieties $\pi_1$ and $\pi_4$ are closer to the center with withdrawing group benzothiadiazole (BTD) relatively, so the conjugated effect between $\pi_1$, $\pi_4$, and A is more strong; therefore, the corresponding interring distances are shortened. In contrast, for $\pi_2$, $\pi_3$, and A, the conjugated effect is not so strong as the former, and the corresponding interring distances are elongated, naturally, by about 0.02 Å.

It can be seen apparently from Table 4 that, in these molecules, the dihedral angles between the two adjacent pieces $\pi$ and A of L-BTD are much smaller than that of other molecules; this may be attributed to the smallest steric hindrance effect of the only linear molecule L-BTD. The dihedral angles between $\pi$ and A for other molecules are quite similar; this can be because the groups connecting to

**Table 3** Selected important interring distances (Å) of the two adjacent moieties D and π, π and A for considered compounds in ground state by MPW1B95/6-31G(d) and HF/6-31G(d) and in excited state by CIS/6-31G(d)

| | Interring distances (Å) | | | | | | | |
|---|---|---|---|---|---|---|---|---|
| | D-$\pi_1$ | $\pi_1$-A | A-$\pi_4$ | $\pi_4$-D | D-$\pi_2$ | $\pi_2$-A | A-$\pi_3$ | $\pi_3$-D |
| MPW1B95/6-31G(d) | | | | | | | | |
| L-BTD | 1.456 | 1.448 | 1.448 | 1.456 | | | | |
| S-BTD | 1.457 | 1.459 | 1.459 | 1.457 | 1.459 | 1.474 | 1.474 | 1.458 |
| S-TBTD | 1.455 | 1.459 | 1.458 | 1.456 | 1.457 | 1.474 | 1.475 | 1.457 |
| S-EBTD | 1.452 | 1.457 | 1.457 | 1.452 | 1.452 | 1.474 | 1.474 | 1.452 |
| S-ABTD | 1.417 | 1.459 | 1.459 | 1.415 | 1.416 | 1.475 | 1.474 | 1.416 |
| S-SBTD | 1.454 | 1.460 | 1.459 | 1.454 | 1.455 | 1.474 | 1.474 | 1.454 |
| S-BTDP | 1.455 | 1.460 | 1.460 | 1.455 | 1.456 | 1.475 | 1.475 | 1.456 |
| HF/6-31G(d) | | | | | | | | |
| L-BTD | 1.476 | 1.470 | 1.470 | 1.476 | | | | |
| S-BTD | 1.477 | 1.482 | 1.482 | 1.477 | 1.477 | 1.492 | 1.492 | 1.478 |
| S-TBTD | 1.476 | 1.482 | 1.482 | 1.476 | 1.477 | 1.492 | 1.492 | 1.477 |
| S-EBTD | 1.474 | 1.482 | 1.482 | 1.474 | 1.474 | 1.492 | 1.492 | 1.474 |
| S-ABTD | 1.438 | 1.483 | 1.483 | 1.438 | 1.438 | 1.492 | 1.492 | 1.438 |
| S-SBTD | 1.475 | 1.483 | 1.483 | 1.475 | 1.475 | 1.492 | 1.492 | 1.475 |
| S-BTDP | 1.475 | 1.483 | 1.483 | 1.475 | 1.475 | 1.492 | 1.492 | 1.475 |
| CIS/6-31G(d) | | | | | | | | |
| L-BTD | 1.459 | 1.420 | 1.420 | 1.459 | | | | |
| S-BTD | 1.461 | 1.435 | 1.435 | 1.460 | 1.477 | 1.490 | 1.490 | 1.478 |
| S-TBTD | 1.471 | 1.435 | 1.434 | 1.471 | 1.476 | 1.490 | 1.490 | 1.477 |
| S-EBTD | 1.461 | 1.434 | 1.434 | 1.461 | 1.474 | 1.490 | 1.490 | 1.474 |
| S-ABTD | 1.430 | 1.435 | 1.435 | 1.430 | 1.438 | 1.491 | 1.491 | 1.438 |
| S-SBTD | 1.472 | 1.434 | 1.436 | 1.473 | 1.475 | 1.490 | 1.490 | 1.475 |
| S-BTDP | 1.459 | 1.435 | 1.435 | 1.459 | 1.475 | 1.490 | 1.490 | 1.475 |

*D* Triphenylamine (2-(pyridin-2-yl)pyridine for S-BTDP)

π π-conjugated bridge

*A* represents Benzothiadiazole

**Table 4** Selected important dihedral angles (°) of the two adjacent moieties D and π, π and A for considered compounds in ground state by MPW1B95/6-31G(d) and HF/6-31G(d) and in excited state by CIS/6-31G(d)

| | Dihedral angles (°) | | | | | | | |
|---|---|---|---|---|---|---|---|---|
| | D-$\pi_1$ | $\pi_1$-A | A-$\pi_4$ | $\pi_4$-D | D-$\pi_2$ | $\pi_2$-A | A-$\pi_3$ | $\pi_3$-D |
| MPW1B95/6-31G(d) | | | | | | | | |
| L-BTD | 14.9 | 16.4 | 18.0 | 14.8 | | | | |
| S-BTD | 20.7 | 35.2 | 37.7 | 22.5 | 10.8 | 62.6 | 63.8 | 12.4 |
| S-TBTD | 23.6 | 37.1 | 36.8 | 19.8 | 29.5 | 64.3 | 68.1 | 29.5 |
| S-EBTD | 4.7 | 32.4 | 32.7 | 3.7 | 5.4 | 61.7 | 67.3 | 0.9 |
| S-ABTD | 92.2 | 39.1 | 33.4 | 46.3 | 51.8 | 65.2 | 66.7 | 0.9 |
| S-SBTD | 6.2 | 37.4 | 37.6 | 3.6 | 10.0 | 70.9 | 66.1 | 3.2 |
| S-BTDP | 26.9 | 38.7 | 38.1 | 26.6 | 18.2 | 64.7 | 63.4 | 22.6 |
| HF/6-31G(d) | | | | | | | | |
| L-BTD | 36.4 | 23.1 | 23.7 | 36.4 | | | | |
| S-BTD | 38.6 | 62.2 | 62.2 | 38.6 | 37.9 | 75.1 | 75.6 | 38.3 |
| S-TBTD | 37.0 | 61.4 | 61.4 | 37.0 | 37.1 | 74.4 | 74.0 | 37.1 |
| S-EBTD | 16.4 | 61.5 | 61.4 | 16.3 | 18.3 | 74.7 | 74.8 | 18.4 |
| S-ABTD | 14.0 | 61.6 | 61.6 | 19.7 | 25.7 | 74.6 | 75.1 | 17.3 |
| S-SBTD | 20.4 | 62.3 | 61.9 | 20.4 | 18.9 | 75.4 | 75.2 | 20.5 |
| S-BTDP | 39.5 | 63.7 | 63.2 | 39.1 | 38.6 | 76.9 | 75.8 | 38.0 |
| CIS/6-31G(d) | | | | | | | | |
| L-BTD | 20.0 | 1.0 | 1.0 | 20.0 | | | | |
| S-BTD | 21.5 | 15.8 | 14.7 | 18.6 | 36.1 | 75.2 | 70.0 | 36.4 |
| S-TBTD | 31.9 | 15.1 | 14.4 | 31.9 | 37.0 | 69.1 | 75.9 | 37.7 |
| S-EBTD | 1.7 | 15.4 | 15.3 | 1.7 | 17.3 | 69.7 | 75.5 | 17.2 |
| S-ABTD | 53.2 | 15.1 | 15.1 | 59.7 | 17.7 | 68.8 | 75.2 | 15.8 |
| S-SBTD | 17.0 | 15.0 | 16.9 | 17.5 | 18.9 | 69.5 | 75.3 | 20.2 |
| S-BTDP | 19.0 | 15.0 | 15.1 | 18.3 | 37.2 | 76.1 | 68.4 | 36.9 |

*D* Triphenylamine (2-(pyridin-2-yl)pyridine for S-BTDP)

π π-conjugated bridge

*A* Benzothiadiazole

center in the π-conjugated bridges are all the same thiophene. The dihedral angles of the two adjacent pieces π and A can also be divided into two groups by the different geometric environment of π-conjugated bridge. Due to larger steric effect, the dihedral angles between $\pi_2$ and A and between $\pi_3$ and A are larger than those of $\pi_1$ and $\pi_4$ accordingly. Compared with π-A, the dihedral angles between the two adjacent moieties π and D do not present very good regularity. First of all, the star-shaped molecule S-BTD has larger steric hindrance effect than the linear molecule L-BTD; the dihedral angles between its π and D are larger than L-BTD, accordingly. However, the dihedral angles between the two adjacent moieties π and D of S-BTDP are larger than those of S-BTD slightly; this may be attributed to that 2-(pyridin-2-yl) pyridine moiety requires for conjugation with the connected group thiophene. Second, the molecule S-TBTD has one more thiophene unit than S-BTD in its π-conjugated bridges, which increase the steric hindrance, resulting in the increase in the dihedral angles between its π and D. Again, the dihedral angles between the two adjacent moieties π and D of the molecules S-EBTD and S-SBTD are significantly smaller than the other molecules; this can be attributed to their small steric hindrance depending on the groups connected to the electron-donor triphenylamine (TPA) in their π-conjugated bridge are all the same vinyl. S-SBTD has one more benzene ring than S-EBTD in the π-conjugated bridges, which enlarge the steric hindrance; as a result, the dihedral angles between its π and D are slightly larger than those of S-EBTD. Finally and most surprisingly, the dihedral angles between π and D of S-ABTD are the largest in all of these molecules; this seems to conflict with the smallest steric hindrance of the acetylene in its π-conjugated bridge that is directly connected to the electron-donor triphenylamine (TPA). However, it must be

noted that the bond lengths between the two adjacent moieties π and D of S-ABTD are also the shortest in all of the considered molecules; this can be attributed to the strong attraction between acetylene group and the lone electron pair on the nitrogen atom of the electron-donor triphenylamine (TPA). It is precisely this strong attraction that leads to the electron-donor triphenylamine (TPA) keep closing to the acetylene group; in this process, the bond length between π and D became shorter and shorter, and the steric hindrance of the electron-donor triphenylamine (TPA) became larger and larger until the dihedral angles were forced to adjust constantly to achieve a balance.

CIS method is still not a bad choice for the intermediate- or large-sized molecules for obtaining excited-state geometry. CIS/6-31G(d) was employed to calculate the lowest singlet excited-state structures based on the optimized geometries obtained from HF/6-31G(d). Some important interring distances and dihedral angles of these molecules in the excited geometries obtained by CIS/6-31G(d) calculations are also listed in Tables 3 and 4.

As can be seen from Tables 3 and 4, although almost all of the interring distances and dihedral angles we concerned are overestimated to some extent by HF method (the dihedral angles between the π-D of S-ABTD is an exception, which are greatly underestimated), the HF calculated results show the same variation with those obtained by the DFT approach in the ground state. So, we can obtain the geometry variation trend from ground state to excited state using the HF and CIS results. As shown in Tables 3 and 4, the electronic excitation leads to the varieties of the star-shaped molecular structures obviously. The interring distance and the dihedral angle between the two adjacent subunits π-D and π-A in the excited states are reduced to some extent. The significant change in the excited-state geometries is mainly in the region between $\pi_1$, $\pi_4$, and A, in which the interring distance is shortened by about 0.05 Å and the dihedral angle decreased by about 47° and 22° for star-shaped and linear molecules. This will undoubtedly increase the conjugated effect. Paradoxically, the dihedral angles of S-ABTD between $\pi_1$, $\pi_4$, and D in the excited states (53.2° and 59.7°) are larger than those in the ground states obtained by the HF approach (14.0° and 19.7°). This can be attributed to the shortest interring distance between $\pi_1$, $\pi_4$, and D, because of which the D units are greatly pulled to the center, so that the dihedral angles are forced to adjust constantly to adapt to the increase in steric hindrance. Overall, the conjugated effect and the local planarity of the singlet excited states are much better than their ground states.

### 3.2 Frontier molecular orbitals

To explore the optical and electronic properties, it is necessary to examine the highest occupied molecule orbital (HOMO), the lowest unoccupied molecule orbital (LUMO), and the energy gap ($\Delta E_{H-L}$), because molecular charge transporting properties are related to the energy and distribution of HOMO and LUMO [26]. A sketch of the HOMOs and LUMOs as well as other important orbitals for studied molecules obtained by MPW1B95/6-31G(d) is provided in in Fig. 3. As shown in Fig. 3, all the frontier orbitals show π characteristics. Both the HOMOs and the LUMOs for studied molecules consist of linear combinations of individual D, π, and A, and π and D groups, respectively. For all of the considered molecules, the HOMOs are spread over the two upper arms (there is no distribution on the thiadiazole unit except S-BTDP) of these molecules, showing a typical D-π-A-π-D structure. However, the LUMOs are centralized mostly on the benzothiodiazole core. Meanwhile, the LUMO + 1 and LUMO + 2 orbitals are spread over the two lower arms and the two upper arms separately (there is no distribution on the four end-groups). This is to say, the electrons mainly transfer from the two end-groups to the electron-withdrawing center of these molecules through their π-conjugated bridge in the transition from HOMO to LUMO. By the same token, the electrons mainly transfer from the two upper arms to the two lower arms in the transition from HOMO to LUMO + 1. Meanwhile, the electrons mainly transfer from both end-groups of the two upper arms and the benzene ring of benzothiadiazole to the π-conjugated bridge and the thiadiazole unit separately in the transition from HOMO to LUMO + 2.

In general, the HOMO exhibits bonding character, and the LUMO has antibonding character. It is noteworthy that the HOMO interaction shows an antibonding between the two adjacent subunits π-A and π-D, and the LUMO represents the bonding interaction in these regions, which is consonant with the shortening of the corresponding interring distance in the discussion for excited states. Importantly, because the lowest singlet excited state corresponds almost exclusively to the excitation from the HOMO to the LUMO in all studied molecules (see the absorption and emission spectra section), we can predict the differences of the bond lengths between the ground ($S_0$) and lowest singlet excited state ($S_1$) from MO nodal patterns. For example, the HOMO orbitals of the studied molecules have nodes between the two adjacent subunits, D and π, and π and A, whereas the LUMO orbitals are bonding in these regions. As a result, we can expect the contraction of these interring bond lengths. The data in Table 3 confirm that these interring bond lengths become considerably shorter in the excited state as discussed earlier.

The HOMO, LUMO energies and energy gaps ($\Delta E_{H-L}$) are listed in Table 5. In theory, the higher the HOMO energy is, the easier to lose the electron, that is easier to produce holes, which makes the molecule have better hole injection ability. On the contrary, the lower the LUMO

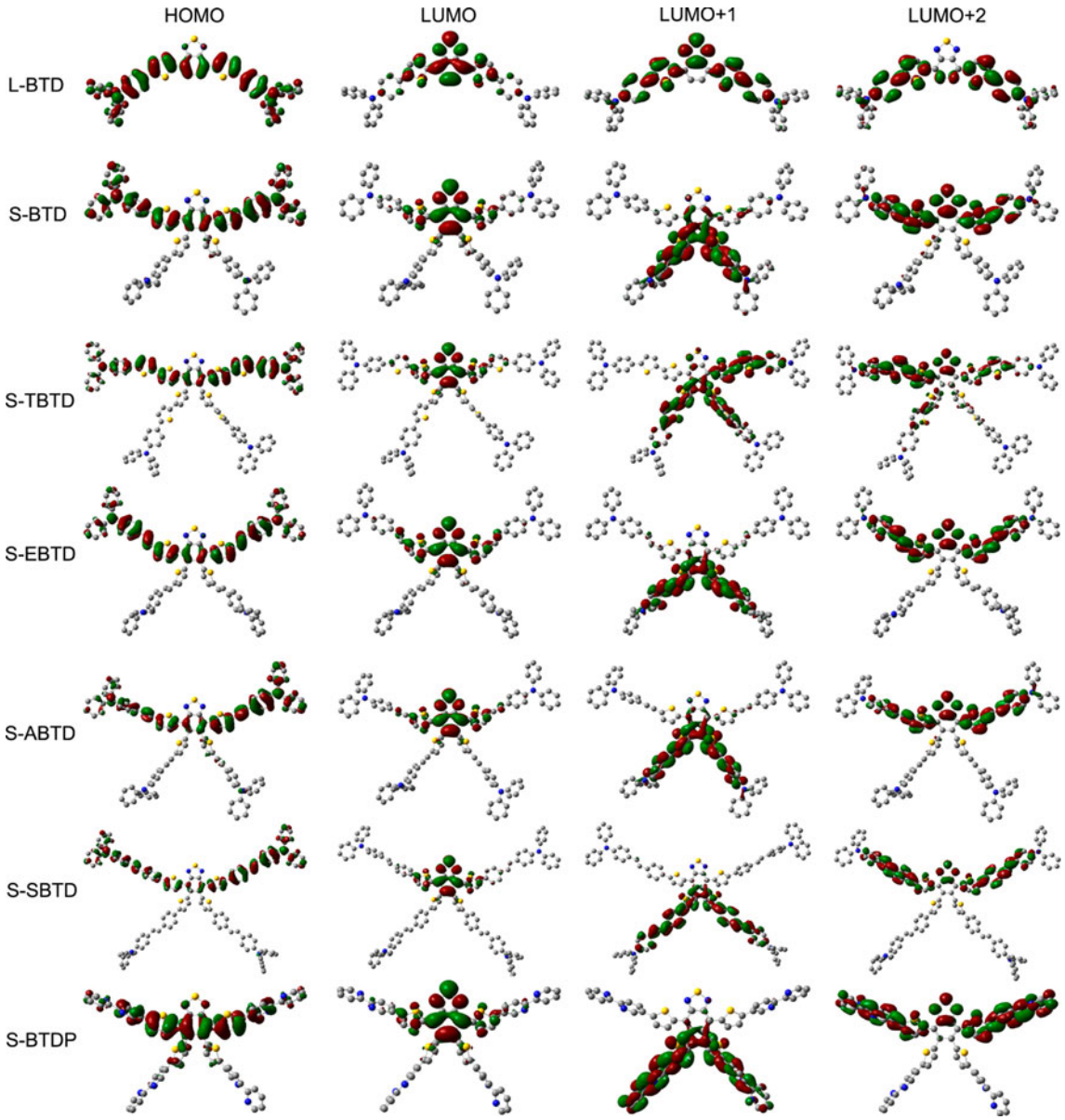


**Fig. 3** Plots of the Frontier Orbitals for the studied molecules by MPW1B95/6-31G(d)

**Table 5** Negative of the HOMO (-εHOMO) and LUMO (-εLUMO) energies, energy gaps for each molecule (in eV) calculated by MPW1B95/6-31G(d)

| Molecule | L-BTD | S-BTD | S-TBTD | S-EBTD | S-ABTD | S-SBTD | S-BTDP |
|---|---|---|---|---|---|---|---|
| -εHOMO | 5.03 | 5.02 | 4.99 | 4.88 | 5.07 | 5.03 | 5.75 |
| -εLUMO | 2.20 | 2.16 | 2.26 | 2.22 | 2.28 | 2.22 | 2.46 |
| $\Delta E_{H-L}$ | 2.83 | 2.86 | 2.73 | 2.66 | 2.79 | 2.81 | 3.29 |

energy is, the easier to accept the electron, which makes the molecule have better electron injection ability. Therefore, it is clearly seen from Table 4 that S-EBTD holding the highest HOMO energy (−4.88 eV) has the strongest hole injection ability in studied molecules. However, S-BTDP holding the lowest LUMO energy (−2.46 eV) has the strongest electron injection ability, indicating that using 2-(pyridin-2-yl) pyridine as end-group can largely improve

**Table 6** Ionization potentials, electron affinities, extraction potentials, and reorganization energies for each molecule (in eV) calculated by MPW1B95/6-31G(d)

| Molecule | IP(v) | IP(a) | HEP | EA(v) | EA(a) | EEP | $\lambda_{hole}$ | $\lambda_{electron}$ |
|---|---|---|---|---|---|---|---|---|
| L-BTD | 5.72 | 5.53 | 5.36 | 1.25 | 1.44 | 1.62 | 0.36 | 0.37 |
| S-BTD | 5.62 | 5.45 | 5.24 | 1.34 | 1.57 | 1.72 | 0.38 | 0.38 |
| S-TBTD | 5.55 | 5.39 | 5.19 | 1.47 | 1.71 | 1.88 | 0.36 | 0.41 |
| S-EBTD | 5.43 | 5.31 | 5.12 | 1.51 | 1.68 | 1.85 | 0.31 | 0.34 |
| S-ABTD | 5.65 | 5.46 | 5.33 | 1.48 | 1.78 | 1.95 | 0.32 | 0.47 |
| S-SBTD | 5.55 | 5.42 | 5.29 | 1.42 | 1.70 | 1.89 | 0.26 | 0.47 |
| S-BTDP | 6.46 | 6.18 | 5.99 | 1.64 | 1.92 | 2.05 | 0.47 | 0.41 |

The suffixes (v) and (a) indicate vertical and adiabatic values, respectively

electron injection ability. In addition, we find that the HOMO, LUMO energies and energy gaps of these molecules are varied, indicating that we can adjust the optical properties of these molecules by changing the nature of their $\pi$-conjugated bridge and end-group.

### 3.3 Ionization potentials and electron affinities

As mentioned in the introduction, we hope improving the electron injection (or transport) properties of studied molecules by changing $\pi$-conjugated bridge or end-group substituent (only for S-BTDP). So it is important to investigate the IPs and EAs, which can be used to evaluate the energy barrier for the injection of holes and electrons. The IPs and EAs calculated by DFT are summarized in Table 6. The IP and EA can be obtained for both vertical excitations (v; at the geometry of the neutral molecule) and adiabatic excitations (a; optimized structure for both the neutral and charged molecule). In addition, HEP is the energy difference from $M^+$ (cationic) to M (neutral molecule) at $M^+$ geometric structure, and EEP is the energy difference from $M^-$ (anionic) to M at $M^-$ geometric structure in the calculation.

As observed from Table 6, all star-shaped molecules (except S-BTDP) hold lower ionization potentials and higher electron affinities than the linear molecule L-BTD; this indicates that the star-shaped molecules we designed have much better hole and electron injection capabilities compared with the linear molecule. Moreover, the molecule S-BTD having the shortest $\pi$-conjugated bridge possess the smallest EA value in these star-shaped molecules, which demonstrate clearly that increasing the length of the $\pi$-conjugated bridge can help to improve the injection capacity of electrons. In the remaining five star-shaped molecules, S-EBTD holds significantly smaller ionization potential (5.31 eV) than the other molecules, indicating that S-EBTD is the best hole injection material. At the same time, S-BTDP holds the largest electron affinity (1.92 eV), so it is the best electron injection material. This is consistent with the conclusion obtained from the analysis for the frontier orbital energy. In the remaining three molecules, S-ABTD has relatively large electron affinity (1.78 eV) and can be used as electron injection material also. S-TBTD and S-SBTD have very similar electron injection ability, but the hole injection ability of the former is slightly stronger than the latter. Based on the above analysis, we can conclude that adding ethylene and more thiophene units to $\pi$-conjugated bridge can effectively improve the IP(a) and EA(a), and adding acetylene and styrene moiety to $\pi$-conjugated bridge can improve EA(a) and have slight adjustment on IP(a). In addition, introducing good electron-acceptor 2-(pyridin-2-yl) pyridine as end-group can significantly improve EA(a), thus, can largely enhance the electron injection ability as we expect.

### 3.4 The charge transport rates and reorganization energies

We have studied the injection ability of holes and electrons of these star-shaped molecules; however, the good charge transfer rate and the comparable balance of charge transfer are also important indicators to evaluate the performance of electroluminescent materials. In general, organic $\pi$-conjugated materials are assumed to transport charge at room temperature via a thermally activated hopping-type mechanism [27–30]. As the vast majority of these organic conductive materials are p-type, the hole-transfer process between adjacent spatially separated segments can be summarized as follows:

$$M^+ + M \rightarrow M + M^+ \quad (1)$$

where M represents the neutral species undergoing charge transfer, and the $M^+$ species contains the hole. If the temperature is sufficiently high to treat vibrational modes classically, then the standard Marcus/Hush model yields the following expression for the hole (or electron) charge transfer rate [31–34].

$$k = \left(\frac{\pi}{\lambda K_b T}\right)^{\frac{1}{2}} \frac{V^2}{\hbar} \exp\left(-\frac{\lambda}{4K_b T}\right) \quad (2)$$

where $T$ is the temperature, $K_b$ is the Boltzmann constant, $\lambda$ is the reorganization energy due to geometric relaxation accompanying charge transfer, and $V$ is the electronic coupling matrix element between the two species, dictated largely by orbital overlap. Obviously, $\lambda$ and $V$ are the two most pivotal parameters and have a dominant impact on the charge transfer rate, especially the former. $V$ usually varies in a small range for the amorphous material. Therefore, our study focused on the reorganization energy of molecules. It

is known that many factors such as solvent polarity, temperature, heteroatom identity, heterocycle substituents, and conjugation chain length will have a significant impact on the reorganization energy. Here, the reorganization energy is just the internal reorganization energy of the isolated active organic $\pi$-conjugated systems due to ignoring any environmental relaxation and changes, i.e., the nuclear configuration changes comprise adjustments in the intramolecular bond lengths and angles. Hence, the reorganization energy for hole and electron transfer in the above equation can be calculated as follows [30]:

$$\lambda_{\text{hole}} = \text{IP}(v) - \text{HEP} \quad (3)$$

$$\lambda_{\text{electron}} = \text{EEP} - \text{EA}(v) \quad (4)$$

It is not difficult to see from Formula 2 that reorganization energy $\lambda$ has a negative index impact on the speed constant $\kappa$ for charge transfer, in other words, the lower the $\lambda$ values, the bigger the charge transport rate. Furthermore, for emitting-layer materials, it needs to achieve the balance between hole and electron transport.

The data in Table 6 show that the $\lambda_{\text{hole}}$ and $\lambda_{e\text{lectron}}$ for L-BTD and S-BTD are very close (even equal) to each other, suggesting that this two molecules have very good charge transfer (or transport) balance performance. S-SBTD holds the smallest $\lambda_{\text{hole}}$ (0.26 eV) and the largest $\lambda_{e\text{lectron}}$ (0.47 eV), can be used as hole transfer (or transport) material (HTM). While S-EBTD (0.31 eV for $\lambda_{\text{hole}}$, 0.34 eV for $\lambda_{e\text{lectron}}$) demonstrated not only faster transport rate of holes and electrons, but also better charge transfer (or transport) balance performance, can be used as emitting-layer material (ELM). It is worth mentioning that 2-(pyridin-2-yl) pyridine as end-group can obviously block the transport of holes; therefore, S-BTDP is suitable to use as electron transport/hole blocking material. In summary, adding ethylene to $\pi$-conjugated bridge can improve both the carrier transport rate and the carrier transport balance. However, adding acetylene, styrene, and more thiophene units to $\pi$-conjugated bridge can only enhance the hole transport rate, but there is disadvantage to the carrier transport balance. Using 2-(pyridin-2-yl) pyridine as end-group cannot improve the transmission performance of carriers.

### 3.5 Absorption spectra

TD MPW1B95/6-31G(d) was employed to investigate the absorption spectra of the studied molecules. The calculated dipole-allowed transitions associated with the maximum absorption wavelengths, oscillator strength ($f$), and transition characters are collected in Table 7, and the experimental absorption maxima are also included. On the basis of the calculation results, simulated electronic absorption spectra are drawn in Fig. 4.

As shown in Table 7 and Fig. 4, all molecules exhibit two absorption bands in the range of 340–410 and 500–613 nm, which are in agreement with the experimental results [12],

**Table 7** Maximal absorption wavelengths (nm) obtained by TDDFT//MPW1B95/6-31G(d) for studied molecules at the MPW1B95/6-31G(d) optimized geometry

| Molecule | Electronic transitions | $\lambda_{\text{max}}^{\text{abs}}$ (nm) | Exp[a] | Exp[b] | $f$ | Main configurations | |
|---|---|---|---|---|---|---|---|
| L-BTD | $S_0 \rightarrow S_1$ | 569.4 | 553 | 533 | 1.0682 | HOMO → LUMO | 0.66 |
| | $S_0 \rightarrow S_4$ | 376.3 | | | 1.2805 | HOMO → LUMO + 1 | 0.63 |
| S-BTD | $S_0 \rightarrow S_1$ | 564.4 | 526 | 500 | 0.5794 | HOMO → LUMO | 0.66 |
| | $S_0 \rightarrow S_9$ | 363.4 | | | 2.1079 | HOMO → LUMO + 2 | 0.52 |
| S-TBTD | $S_0 \rightarrow S_1$ | 590.5 | 553 | 530 | 0.9538 | HOMO → LUMO | 0.65 |
| | $S_0 \rightarrow S_7$ | 403.8 | | | 1.3656 | HOMO → LUMO + 2 | 0.41 |
| | | | | | | HOMO → LUMO + 1 | 0.40 |
| | $S_0 \rightarrow S_{10}$ | 390.9 | | | 1.4755 | HOMO-7 → LUMO | 0.35 |
| S-EBTD | $S_0 \rightarrow S_1$ | 612.8 | | | 0.9010 | HOMO → LUMO | 0.66 |
| | $S_0 \rightarrow S_7$ | 409.5 | | | 0.9215 | HOMO → LUMO + 1 | 0.53 |
| | $S_0 \rightarrow S_9$ | 402.9 | | | 2.6414 | HOMO → LUMO + 2 | 0.56 |
| S-ABTD | $S_0 \rightarrow S_1$ | 572.3 | | | 0.8347 | HOMO → LUMO | 0.66 |
| | $S_0 \rightarrow S_8$ | 382.9 | | | 1.6093 | HOMO → LUMO + 1 | 0.40 |
| | $S_0 \rightarrow S_9$ | 376.9 | | | 2.1551 | HOMO → LUMO + 2 | 0.51 |
| S-SBTD | $S_0 \rightarrow S_1$ | 555.8 | | | 0.9650 | HOMO → LUMO | 0.62 |
| | $S_0 \rightarrow S_8$ | 405.6 | | | 2.0510 | HOMO → LUMO + 1 | 0.27 |
| | $S_0 \rightarrow S_9$ | 402.0 | | | 3.5848 | HOMO → LUMO + 2 | 0.50 |
| S-BTDP | $S_0 \rightarrow S_1$ | 500.3 | | | 0.6139 | HOMO → LUMO | 0.67 |
| | $S_0 \rightarrow S_6$ | 346.3 | | | 0.6352 | HOMO → LUMO + 2 | 0.55 |
| | $S_0 \rightarrow S_7$ | 340.7 | | | 1.4686 | HOMO-1 → LUMO + 1 | 0.51 |

[a] Measured in thin film [12]

[b] Measured in THF [12]

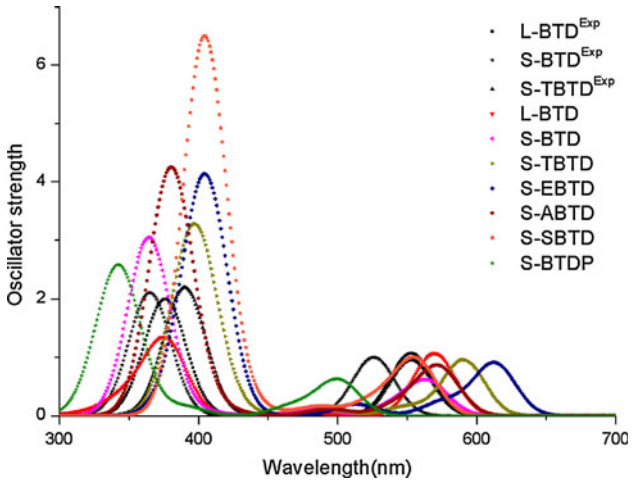


**Fig. 4** Simulated electronic absorption spectra of the studied molecules with the calculated data by TD MPW1B95/6-31G(d) (*in colorful line*) and with experimental data (*in black line*)

especially the band located at shorter wavelength. The absorption peaks located at 340–410 nm can be assigned to $\pi$–$\pi^*$ transitions and are stronger than the one at 500–613 nm for star-shaped molecules, which is caused by the absorption of the substituents at the 5 and 6 positions of benzothiadiazole. Also, the visible absorption peaks located around 500–613 nm resulted from intramolecular charge transfer (ICT) from the donor (TPA) to the acceptor (BTD).

Obviously, the excitation to the $S_1$ state corresponds all exclusively to the promotion of an electron from HOMO to LUMO. As listed in Table 7, the absorption spectra of $S_1$ located at 569.4, 564.4, 590.5, 612.8, 572.3, 555.8, and 500.3 nm for L-BTD, S-BTD, S-TBTD, S-EBTD, S-ABTD, S-SBTD, and S-BTDP, respectively. This is reasonable because the HOMO → LUMO transition is predominant in the $S_0 \rightarrow S_1$ electronic transition and, as the analysis for $\Delta E_{H-L}$ above, with the introduction of the different $\pi$-conjugated bridge and end-group, the HOMO–LUMO gaps changed. The largest oscillator strengths of L-BTD correspond to the $S_0 \rightarrow S_4$ electronic transitions, those of S-TBTD and S-BTDP correspond to the $S_0 \rightarrow S_7$ electronic state transitions. For other molecules, the largest oscillator strengths, however, correspond to the $S_0 \rightarrow S_9$ electronic transitions. All of these electronic transitions are from HOMO (HOMO-1 for S-BTDP) to LUMO + 1/LUMO + 2, and this may be attributed to the change in the local electron density distribution (see Fig. 3).

### 3.6 Emission spectra

Based on the excited-state geometries optimized by ab initio CIS/6-31G(d), TDDFT was used to predict emission spectra. The calculated results together with the experimental spectra are summarized in Table 8. On the basis of the calculation results, simulated electronic emission spectra are drawn in Fig. 5. The emission peaks arising from $S_1$ to $S_0$ of these molecules are all assigned to $\pi$–$\pi^*$ character. The emission wavelength of L-BTD, S-BTD, and S-TBTD obtained by TDDFT is smaller than available experimental data by 48, 17, and 31 nm, respectively, which is considered in good agreement with the experimental values [12]. The large Stokes shifts ranging from 79 to 119 nm may be explained by a significant geometry deform on going from the ground state to the excited state of the considered molecules [35]. Most importantly, the emission wavelengths of these molecules are all in the range of 619–706 nm, which is entirely included in the range of red light-emitting wavelength, indicating that these molecules can be used as red light-emitting material.

The radiative lifetimes ($\tau$) calculated for spontaneous emission are also calculated using the Einstein transition probabilities according to the following formula (in au) [36, 37], and the results are included in Table 8.

$$\tau = c^3/2(E_{\mathrm{Flu}})^2 f$$

where $c$ is the velocity of light, $E_{\mathrm{Flu}}$ is the transition energy, and $f$ is the oscillator strength. The data of $f$ and $\tau$ are also shown in Table 8. The calculated radiative lifetimes of L-BTD, S-BTD, S-TBTD, S-EBTD, S-ABTD, S-SBTD, and S-BTDP are 5.33, 6.61, 5.08, 5.72, 5.36, 4.74, and 5.63 ns, respectively. The compounds S-BTD have the longest radiative lifetime than the others in this study due to its largest Stokes shift [38].

Electroluminescence in organic light-emitting diodes arises from a charge transfer reaction between the injected positive and negative charges by which they combine to form excitons (hole–electron pair that combined by Coulomb interaction, and this Electrostatic Coulomb force is called exciton binding energy Eb) that subsequently decay radiatively. The quantum yield of this process (the number of photons generated per electron or hole injected) is often thought to have a statistical upper limit of 25%. This is based on the assumption that the formation cross-section of singlet excitons $\sigma_S$ is approximately the same as that of any one of the three equivalent nonradiative triplet exciton states $\sigma_T$, that is, $\sigma_S/\sigma_T = 1$, then the singlet generation fraction $\chi_S = \sigma_S/(\sigma_S + \sigma_T)$ will be limited to 25% by the degeneracy of the triplets [39–41]. However, the recent experimental maximum internal quantum efficiency (IQE) of OLEDs has exceeded the theoretical statistical upper limit of 25% [42–45]. And the high singlet-to-triplet exciton-formation cross-section ratio ($\sigma_S/\sigma_T$) in conjugated systems is believed to be a possible reason for the high IQE. Theoretically, Shuai et al. [46] have first suggested that exciton-formation rates are different for different spin

**Table 8** Emission data obtained by TDDFT//MPW1B95/6-31G(d) for studied molecules at the CIS/6-31G(d) optimized geometry

| Molecule | Electronic transitions | $\lambda_{max}^{em}$ (nm) | Exp[a] | $f$ | Main configurations | | $\tau$ (ns) | $E_{bS}$ (eV) | $E_{bT}$ (eV) | $\sigma_S/\sigma_T$ | $\chi_s$ |
|---|---|---|---|---|---|---|---|---|---|---|---|
| L-BTD | $S_1 \rightarrow S_0$ | 648 | 696 | 1.1869 | HOMO → LUMO | 0.63 | 5.33 | 0.92 | 1.90 | 2.07 | 0.41 |
| S-BTD | $S_1 \rightarrow S_0$ | 673 | 690 | 1.0326 | HOMO → LUMO | 0.70 | 6.61 | 1.02 | 1.91 | 1.87 | 0.38 |
| S-TBTD | $S_1 \rightarrow S_0$ | 689 | 720 | 1.4035 | HOMO → LUMO | 0.70 | 5.08 | 0.93 | 1.82 | 1.96 | 0.39 |
| S-EBTD | $S_1 \rightarrow S_0$ | 706 | | 1.3030 | HOMO → LUMO | 0.70 | 5.72 | 0.50 | 1.38 | 2.76 | 0.48 |
| S-ABTD | $S_1 \rightarrow S_0$ | 676 | | 1.2871 | HOMO → LUMO | 0.70 | 5.36 | 0.83 | 1.71 | 2.06 | 0.41 |
| S-SBTD | $S_1 \rightarrow S_0$ | 659 | | 1.3779 | HOMO → LUMO | 0.63 | 4.74 | 0.93 | 1.83 | 1.97 | 0.40 |
| S-BTDP | $S_1 \rightarrow S_0$ | 619 | | 1.0235 | HOMO → LUMO | 0.63 | 5.63 | 1.29 | 2.29 | 1.78 | 0.37 |

[a] Measured in thin film excited at 520 nm [12]

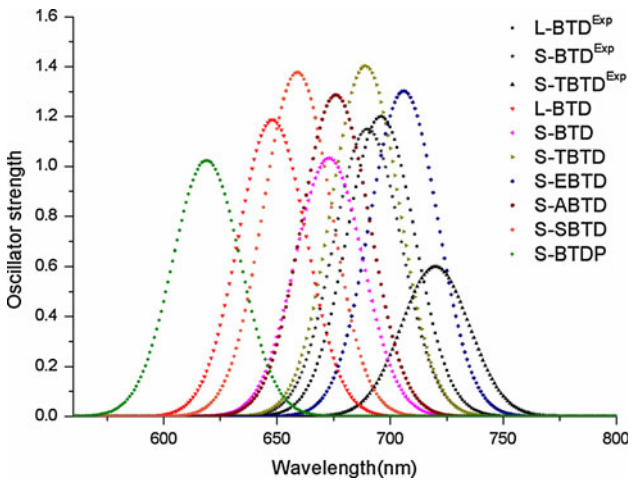


**Fig. 5** Simulated electronic emission spectra of the studied molecules with the calculated data by TD MPW1B95/6-31G(d) (*in colorful line*) and with experimental data (*in black line*)

manifolds. They pointed out that electron–phonon coupling (exciton-binding energy dissipation process) is important for the exciton formation to be spin dependent. Later, Karabunarliev and Bittner have further explored this issue and found that the formation rate can be simply expressed as inversely proportional to the exciton binding energy [40]. Recently, by following Karabunarliev and Bittner and Shuai et al. [47, 48], Huang et al. [49] calculated the singlet exciton-formation fractions ($\chi_S$), and the ratio $\sigma_S/\sigma_T$ of the formation cross-section of the singlet and triplet is

$$\sigma_S/\sigma_T = E_{bT}/E_{bS}$$

where $\sigma_S$ and $\sigma_T$ represent the formation cross-sections of singlet and triplet excitons, and $E_{bS}$ and $E_{bT}$ are the binding energies of the singlet and triplet excitons, respectively. $E_{bS}$ and $E_{bT}$ can be calculated as

$$E_{bS} = \Delta E_{H-L} - E_{S1}$$

$$E_{bT} = \Delta E_{H-L} - E_{T1}$$

where $\Delta E_{H-L}$ is the HOMO-LUMO energy gap. $E_{S1}$ and $E_{T1}$ are excitation energies from the ground state to the lowest excited singlet state and the lowest excited triplet state, respectively.

Based on the above considerations, we calculated the exciton binding energy ($E_{bS}$ and $E_{bT}$), the singlet-to-triplet exciton-formation cross-section ratio ($\sigma_S/\sigma_T$) and the singlet exciton generation fraction ($\chi_S$) of the molecules in this study, and the data are also shown in Table 8. As can be seen in Table 8, for the star-shaped molecules S-EBTD, S-ABTD, and S-SBTD, the calculated formation cross-section ratios of singlet over triplet excitons ($\sigma_S/\sigma_T$) are 2.76, 2.06. 1.97, respectively, with corresponding singlet exciton-formation fractions ($\chi_S$) of 0.48, 0.41, and 0.40, which are higher than those of the experimental molecules S-BTD ($\sigma_S/\sigma_T = 1.87$, $\chi_S = 0.38$) and S-TBTD ($\sigma_S/\sigma_T = 1.96$, $\chi_S = 0.39$), suggesting their potential as the highly efficient fluorescent-light-emitting materials, especially for S-EBTD. For L-BTD and S-BTDP, the calculated formation cross-section ratios of singlet over triplet excitons ($\sigma_S/\sigma_T$) are 2.07 and 1.78, and the corresponding singlet exciton-formation fractions ($\chi_S$) are 0.41 and 0.37.

## 4 Conclusions

A comprehensive theoretical investigation on the star-shaped molecules with the typical D-π-A-π-D push–pull structure has been performed. The calculated results show that the carrier injection and transport ability of these molecules are largely tuned by the π-conjugated bridge and the end-group. For our designed molecules S-BTDP, S-EBTD, and S-SBTD, S-BTDP has the lowest LUMO energy (−2.46 eV) and the largest EA(a) (1.92 eV), indicating that it can be used as excellent electron injection and hole blocking material. However, S-EBTD has the highest HOMO energy (−4.88 eV) and the smallest IP(a) (5.31 eV), which can be used as excellent hole injection material. More than that, the $\lambda_{hole}$ (0.31 eV) and

$\lambda_{electron}$ (0.34 eV) of S-EBTD are small and close to each other, indicating that it has not only faster transport rate of hole and electron, but also better charge transfer balance; thus, it also can be excellent light-emitting material. Meanwhile, S-SBTD with the smallest $\lambda_{hole}$ (0.26 eV) can be used as hole transport material. In summary, we can conclude that using ethylene as π-conjugated bridge can effectively improve both the hole injection and carrier transport ability, introducing 2-(pyridin-2-yl) pyridine as end-group can significantly increase the ability of electron injection, and adding styrene moiety to π-conjugated bridge can enhance hole transport rate. Moreover, the formation cross-section ratios of singlet over triplet excitons and the exciton-formation rate of these molecules are in the range of 1.78–2.76 and 0.37–0.48, respectively. It is suggesting that they have great potential for applications as efficient fluorescent-light-emitting materials. In addition, the radiative lifetime of these compounds is within the range from 4.74 to 6.67 ns. The absorption spectra of these molecules show two absorption bands in the range of 340–410 and 500–613 nm, respectively, which are in agreement with the experimental results. The emission wavelengths of these compounds fall into red range, implying that they can be used as red light-emitting materials.

**Acknowledgments** This work is supported by the Major State Basic Research Development Program (2002CB 613406), the National Natural Science Foundation of China (Project No. 20973078), the State Key Laboratory of Theoretical and Computational Chemistry of Jilin University.

## References

1. Yang Y, Zhou Y, He QG, He C, Yang CH, Bai FL, Li YF (2009) J Phys Chem B 113:7745
2. Shirota Y, Kageyama H (2007) Chem Rev 107:953
3. Tang RP, Tan ZA, Li YF, Xi F (2006) Chem Mater 18:1053
4. Chen CT (2004) Chem Mater 16:4389
5. Ren XF, Ren AM, Feng JK, Zhou X (2010) Org Electron 11:979
6. Wu WC, Yeh HC, Chan LH, Chen CT (2002) Adv Mater 14:1072
7. Thomas KRJ, Lin JT, Tao YT, Chuen CH (2002) Adv Mater 14:822
8. Liu J, Shao SY, Chen L, Xie ZY, Cheng YX, Geng YH, Wang LX, Jing XB, Wang FS (2007) Adv Mater 19:1859
9. Luo J, Li XZ, Hou Q, Peng JB, Yang W, Cao Y (2007) Adv Mater 19:1113
10. Ma XM, Hua JL, Wu WJ, Jin YH, Meng FS, Zhan WH, Tian H (2008) Tetrahedron 64:345
11. Du JP, Xu EJ, Zhong HL, Yu F, Liu C, Wu HR, Zeng DL, Ren SJ, Sun J, Liu YC, Cao AM, Fang Q (2008) J Polym Sci Polym Chem Ed 46:1376
12. Li WW, Du C, Li FH, Zhou Y, Fahlman M, Bo ZS, Zhang FL (2009) Chem Mater 21:5327
13. He C, He QG, Yi YP, Wu GL, Bai FL, Shuai ZG, Li YF (2008) J Mater Chem 18:4085
14. Ma CQ, Fonrodona M, Schikora MC, Wienk MM, Janssen RAJ, Bäuerle P (2008) Adv Funct Mater 18:3323
15. Fischer MKR, Ma CQ, Janssen RAJ, Debaerdemaeker T, Bäuerle P (2009) J Mater Chem 19:4784
16. Kopidakis N, Mitchell WJ, Lagemaat JVD, Ginley DS, Rumbles G, Shaheen SE, Rance WL (2006) Appl Phys Lett 89:103524
17. Lee TW, Kim DC, Kang NS, Yu JW, Cho MJ, Kim KH, Choi DH (2008) Chem Lett 37:866
18. Kim YG, Christian PH, Ananthakrishnan N, Niazimbetova ZI, Thompson BC, Galvin ME, Reynolds JR (2008) Sol Energy Mater Sol Cells 92:307
19. Alévêque O, Leriche P, Cocherel N, Frère P, Cravino A, Roncali J (2008) Sol Energy Mater Sol Cells 92:1170
20. Cravino A, Roquet S, Alévêque O, Leriche P, Frère P, Roncali J (2006) Chem Mater 18:2584
21. Roncali J, Frère P, Blanchard P, Bettignies RD, Turbiez M, Roquet S, Leriche P, Nicolas Y (2006) Thin Solid Films 511–512:567
22. Zhang XW, Li J, Khan MA, Zhang L, Jiang XY, Khizar-ul H, Zhu WQ, Zhang ZL (2009) Semicond Sci Technol 24:075021
23. Sousa SF, Fernandes PA, Ramos MJ (2007) J Phys Chem A 111:10439
24. Zhao Y, Truhlar DG (2004) J Phys Chem A 108:6908
25. Frisch MJ, Trucks GW, Schlegel HB, Scuseria GE, Robb MA, Cheeseman JR, Montgomery JA Jr, Vreven T, Kudin KN, Burant JC, Millam JM, Iyengar SS, Tomasi J, Barone V, Mennucci B, Cossi M, Scalmani G, Rega N, Petersson GA, Nakatsuji H, Hada M, Ehara M, Toyota K, Fukuda R, Hasegawa J, Ishida M, Nakajima T, Honda Y, Kitao O, Nakai H, Klene M, Li X, Knox JE, Hratchian HP, Cross JB, Bakken V, Adamo C, Jaramillo J, Gomperts R, Stratmann RE, Yazyev O, Austin AJ, Cammi R, Pomelli C, Ochterski JW, Ayala PY, Morokuma K, Voth GA, Salvador P, Dannenberg JJ, Zakrzewski VG, Dapprich S, Daniels AD, Strain MC, Farkas O, Malick DK, Rabuck AD, Raghavachari K, Foresman JB, Ortiz JV, Cui Q, Baboul AG, Clifford S, Cioslowski J, Stefanov BB, Liu G, Liashenko A, Piskorz P, Komaromi I, Martin RL, Fox DJ, Keith T, Al-Laham MA, Peng CY, Nanayakkara A, Challacombe M, Gill PMW, Johnson B, Chen W, Wong MW, Gonzalez C, Pople JA (2004) Gaussian 03, revision C.02. Gaussian Inc, Wallingford
26. Chu TY, Ho MH, Chen JF, Chen CH (2005) Chem Phys Lett 415:137
27. Epstein AJ, Lee WP, Prigodin VN (2001) Synth Met 117:9
28. Reedijk JA, Marten HCF, van Bohemena SMC, Hilt O, Brom HB, Michelsb MAJ (1999) J Synth Met 101:475
29. Mott NF, Davis EA (1979) Electronic processes in non-crystalline materials, 2nd edn. Oxford University Press, Oxford
30. Hutchison GR, Ratner MA, Marks TJ (2005) J Am Chem Soc 127:2339
31. Marcus RA (1993) Rev Mod Phys 65:599
32. Marcus RA, Eyring H (1964) Annu Rev Phys Chem 15:155
33. Hush NS (1958) J Chem Phys 28:962
34. Marcus RA (1956) J Chem Phys 24:966
35. Chernyak V, Meier T, Tsiper E, Mukamel S (1999) J Phys Chem A 103:10294
36. Barzilai IL, Bulatov V, Schechter I (2004) Anal Chim Acta 501:151
37. Lukeš V, Aquino A, Lischka H (2005) J Phys Chem A 109:10232
38. Zou LY, Ren AM, Feng JK, Ran XQ (2009) J Phys Org Chem 22:1104
39. Wohlgenannt M, Kunj T, Mazumdar S, Ramasesha S, Vardeny ZV (2001) Nature 409:494
40. Karabunarliev S, Bittner ER (2003) Phys Rev Lett 90:057402
41. Wohlgenannt M, Jiang XM, Vardeny ZV, Janssen RAJ (2002) Phys Rev Lett 88:197401
42. Baldo MA, O'Brien DF, Thompson ME, Forrest S (1999) Phys Rev B 60:14422

43. Ho PKH, Kim JS, Burroughes JH, Becker H, Li SFY, Brown TM, Cacialli F, Friend RH (2000) Nature 404:481
44. Cao Y, Parker ID, Yu G, Zhang C, Heeger AJ (1999) Nature 397:414
45. Wilson JS, Dhoot AS, Seeley AJAB, Khan MS, Köhler A, Friend RH (2001) Nature 413:828
46. Shuai Z, Beljonne D, Silbey RJ, Brédas JL (2000) Phys Rev Lett 84:131
47. Chen LP, Zhu LY, Shuai ZG (2006) J Phys Chem A 110:13349
48. Yin SW, Chen LP, Xuan PF, Chen KQ, Shuai Z (2004) J Phys Chem B 108:9608
49. Yin J, Chen RF, Zhang SL, Ling QD, Huang W (2010) J Phys Chem A 114:3655